33rd EPS Conference on Plasma Phys. Rome, 19 - 23 June 2006 ECA Vol.**30I**, P-5.137 (2006)

Predictive Modeling of Plasma Halo Evolution in Post-Thermal Quench Disrupting Plasmas

D.A. Humphreys,[1] D.G. Whyte,[2] M. Bakhtiari,[2] R.D. Deranian,[1] E.M. Hollmann,[3] A.W. Hyatt,[1] T.C. Jernigan,[4] A.G. Kellman[1] and P.B. Parks[1]

[1]*General Atomics, P.O. Box 85608, San Diego, California 92186-5608, USA*
[2]*University of Wisconsin-Madison, Madison, Wisconsin*
[3]*University of California-San Diego, La Jolla, California*
[4]*Oak Ridge National Laboratory, Oak Ridge, Tennessee*

I. Introduction

Halo currents flowing on open field lines when the plasma boundary is in contact with the wall during a disruption current quench (CQ) can apply large forces to conducting structure and plasma facing components (PFCs). Successful models of halo and core plasma current evolution developed in the last decade account for many of the relevant processes and allow prediction of halo currents provided the post-thermal quench (TQ) core and halo resistivities and halo width evolution are given [1-4]. Key elements lacking predictability have remained halo width evolution, effectiveness of impurity penetration, and impurity species concentrations in the post-TQ plasma. Analysis of DIII-D data suggests that the effective halo width is set by the plasma motion and natural current diffusion across open field lines in the post-TQ plasma.

II. Physics of VDE Plasma/Halo Evolution

The axisymmetric component of the halo current is driven by convection and induction from the plasma core which is described by a model using a coupled set of differential circuit equations for the evolution of the core current, I_p, and the toroidal halo current, $I_{h(tor)}$ [2,4]. The total toroidal halo current is related to the total poloidal halo current via $I_{h(pol)} = I_{h(tor)}/q_h$, where q_h is the effective halo safety factor.

The model accurately describes the evolution of core and halo plasma currents during mitigated and unmitigated disruptions in DIII-D, provided the core plasma resistivity and the ratio of halo resistivity to halo width are specified correctly. Implications include:

- The ratio of the peak halo current to the initial plasma current increases both with the ratio of the vertical instability growth rate to the core current decay rate, and the ratio of core and halo current decay rates.
- Single constant values of both the core resistivity and the halo resistivity-to-width ratio are sufficient to reproduce typical vertical displacement events (VDEs).
- "Type I" VDEs occur when the growth rate is smaller than the core current decay rate so that the halo safety factor remains high, and the poloidal halo current stays relatively low. "Type II" VDEs occur when the growth rate is larger than the core current decay rate so that the halo safety factor drops to unity (but is always prevented from dropping lower by MHD activity), producing the highest attainable poloidal halo current for a given toroidal halo current. The highest peak halo current fractions in DIII-D therefore occur in Type II VDEs. The lowest peak halo current fractions occur in VDEs converted to Type I through radiative cooling by massive injection of impurity gases such as Ne [5].

III. Analysis of Halo Width Evolution in DIII-D VDEs

The DIII-D tile current array (TCA) includes a set of six floor tiles instrumented to measure total (poloidal) current flowing in each tile from the plasma-facing side to the vessel. We define the TCA halo width as the poloidal current-weighted distance from the contact point

$$w_{halo}(TCA) \equiv \frac{1}{I_h^{pol}} \int_0^{R_{wall}} J_h^{pol} 2\pi R dR \quad , \tag{1}$$

where the poloidal halo current density J_h^{pol} is a function of position from the contact point to the inboard wall. This definition produces a halo width value corresponding to the width at half-maximum for a linearly decreasing profile. Figure 1 shows the history of a typical Ne gas-mitigated VDE. Figure 1(a) shows the total plasma current (core + halo; solid line) and the core current alone (dashed) during the CQ. Figure 1(b) shows the total poloidal halo current measured by the TCA (solid) and inferred from the JFIT magnetic reconstruction algorithm (dashed) [4]. Figure 1(c) shows the TCA halo width (solid line), which increases steadily throughout but is fairly constant during the CQ. The dashed line indicates the distance from the inboard wall to the last closed flux surface (LCFS) measured at the plasma midplane. This dimension is typically less than the halo width at the TCA due to flux expansion near the floor. Figure 1(d) shows the decreasing minor radius of the core plasma LCFS as the plasma moves into the floor. Figure 1(e) shows the halo safety factor (at LCFS), which remains high (well above unity) during the CQ, limiting the amplitude of the poloidal halo current. This disruption is therefore a Type I VDE, in which the current decay time is shorter than the vertical motion time. Although the halo model is expressed in terms of core-halo induction, the process can also be described in terms of current diffusion. The relatively cold, high resistivity halos that characterize Type I VDEs produce rapid diffusion across the open field lines. Application of the halo model to the discharge of Fig. 1 yields core and halo electron temperatures of 5.0 eV (assuming $Z_{eff} = 1$), constant throughout the CQ. The timescale for current diffusion into a halo of this resistivity $\eta_h = 7.0\times10^{-5}$ ohm-m and width $\delta_h = 0.2$ m, when the core plasma has minor radius $a = 0.4$ m, is given by $\tau_{diff} \approx \mu_0\, a\, \delta_h/\eta_h \sim 1.4$ ms, less than the 4 ms duration of the CQ in this case. The TCA halo width $w_{halo} \sim 0.22$ m in this discharge corresponds to current which has diffused to contact the inboard wall (0.4 m from the contact point), and suggests that this may commonly occur in Type I VDEs.

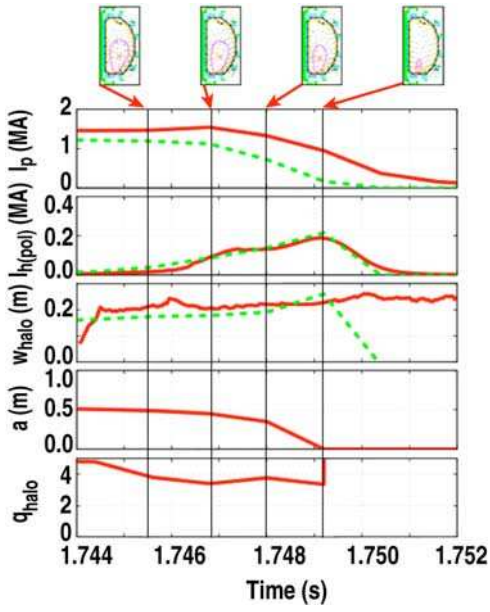

Fig. 1. Disruption history and halo evolution in Ne-mitigated VDE (#110217).

In order to compare the halo widths in many discharges, we define a single scalar quantity to characterize the halo width across the CQ as the TCA halo width averaged over the duration of the CQ, weighted by the total poloidal halo current

$$\langle w_{halo}(TCA) \rangle \equiv \frac{\int_{CQ} w_{halo}(t) I_{h(pol)}(t) dt}{\int_{CQ} I_{h(pol)}(t) dt} \quad . \tag{2}$$

This average emphasizes the halo width near the time of peak halo current. Figure 2 compares values of $\langle w_{halo}(\mathrm{TCA})\rangle$ for a set of DIII-D VDEs as a function of poloidal halo current fraction (which reflects the core-halo resistivity ratio and distinguishes the Type I and II VDE regimes). The figure shows that halo widths lie in the range of 0.20–0.27 for a representative set of DIII-D VDEs, consistent with halos whose currents have generally diffused to the inboard wall of DIII-D. However, the correlation of wider halos with lower halo fractions (and thus colder halos, Type I VDEs) and narrower halos with higher halo fractions (and thus hotter halos, Type II VDEs) seen in the figure is significant. To see this, we analyze exemplars of each VDE class in some detail using magnetic reconstruction with the JFIT code.

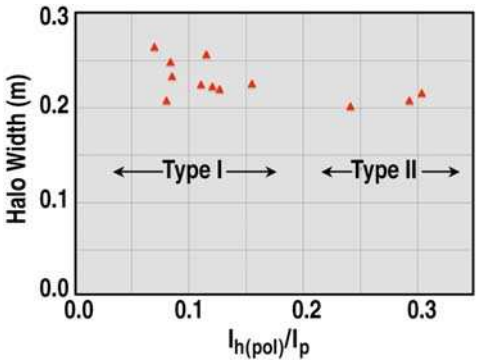

Fig. 2. Summary of halo widths in DIII-D VDEs.

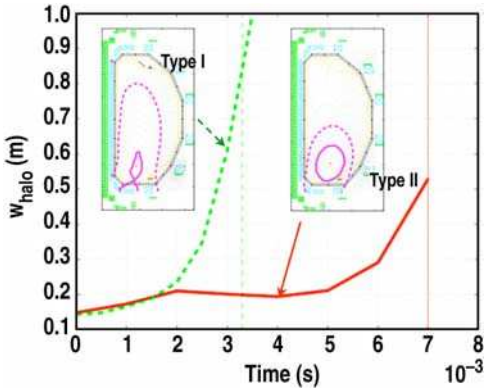

Fig. 3. Comparison of halo geometries in examples of Type I and Type II VDEs.

The JFIT code reconstructs the current density distribution across core and halo regions of plasma. Halo currents derived from JFIT agree well with TCA measurements [4]. JFIT identifies the core (LCFS) and halo regions, and can estimate the edge of the halo region. Figure 3 shows halo width evolution data from JFIT reconstructions in two discharges: a Type I VDE produced by massive injection of ~1400 torr-l of Ne gas (#110216; dashed line), and a Type II "natural" VDE (#93204; solid line). The JFIT estimate of halo width is a local toroidal halo current-weighted average in the entire non-core plasma region [similar to Eq. (1)]. The time axes in Fig. 3 are shifted so that $t = 0$ corresponds to the start of each CQ. JFIT reconstructions are shown for the two discharges at times indicated by arrows, corresponding to points when the core plasma has moved ~1 m downward and near the end of the core current in both cases. The absolute edge of the halo, defined as the flux surface enclosing 90% of the total halo current, is marked by a dashed line for reference [note that this defines a region approximately twice the current-weighted halo width defined by Eq. (2)]. The reconstructions show that the halo current has diffused to the inboard wall (particularly in the vicinity of the floor tiles) in both cases. However, the halo current has moved downward along with the core plasma in the Type II case (remaining narrow), but has diffused significantly away from the edge of the core in the Type I case. This is consistent with a colder halo (and core) in Type I VDEs relative to Type II. The time traces show this greater diffusion distance in the Type I case as well, but also show that the halo width varies slowly and relatively little across the time during which most of the core current is lost, (0–2.0 ms for Type I; 0–5.0 ms for Type II) indicating that fixing the halo width at a constant spatial value allows simulations to accurately reproduce halo current evolution in DIII-D.

From halo model simulations, the core and halo electron temperatures are inferred to be 2.0 eV (assuming Z_{eff} =1) in the Fig. 3 Type I case, corresponding to a characteristic time of ~2.0 ms for the halo current to diffuse 1.0 m, the distance shown in Fig. 3. This is somewhat

shorter than the CQ time of ~3.5 ms in the Type I case. By contrast, core and halo electron temperatures of approximately 16 eV in the Type II case yield a characteristic diffusion time of 8.4 ms for the halo current to diffuse the same distance, somewhat longer than the CQ time of ~ 6 ms. Since the halo current continues to move vertically with the core current during the VDE, the slower diffusion rate cannot overcome this motion to expand the halo region appreciably (until the LCFS is gone and the motion ends).

That halo currents can freely diffuse to PFC surfaces is consistent with observations that current-carrying plasma is present up to such surfaces, even during a discharge flattop. Typical electron temperatures in this far scrapeoff layer region are observed to be on the order of 1-2 eV, comparable to post-TQ temperatures in mitigated disruptions [6]. Assumption of such a potentially current-carrying plasma throughout the machine aperture is the key element required for predictive modeling and simulation of disruptions to guide device designs.

The KPRAD code is a 0-D time-dependent impurity radiation and ionization code with self-consistent energy balance including radiation losses, ionization and recombination of all species, collisional coupling, and ohmic heating. When the plasma is dominated by a known impurity species (as in disruption mitigation by massive gas injection), the code determines post-TQ conditions very accurately [3,4]. KPRAD calculations T_e = 2.2 eV with Z_{eff} of 1.0 for the mitigated (Type I) VDE of Fig. 3 agree closely with the values inferred from the halo model (T_e = 2.0 eV, Z_{eff} = 1.0). Post-TQ conditions determined by "natural" sources of impurity content in unmitigated VDEs have proven much more difficult to predict, which underscores the importance of massive impurity mitigation for devices such as ITER.

IV. Summary and Conclusions

The halo width in a post-TQ VDE appears to be set by the competing processes of motion and diffusion of the current from core to machine wall. Colder plasmas (Type I, current decay-dominated VDEs) permit rapid diffusion relative to the timescale of the CQ, and thus produce wide halos by time the LCFS is lost. Hotter plasmas (Type II, motion-dominated VDEs) limit the diffusion rate on the timescale of the CQ, and thus produce relatively narrow halos through the time of peak halo current. The characteristic halo width is also typically limited by machine geometry. The net result of these effects is to allow a single scalar value to represent the effective halo width in DIII-D VDEs. In general, however, a detailed code must simulate this diffusion to calculate the evolution of the halo geometry. The present analysis of halo evolution physics processes provides a firm basis for such simulations to assume the presence of halo plasma throughout the vessel from the beginning of the CQ.

Acknowledgment

This work supported by the U.S. Department of Energy under DE-FC02-04ER54698, DE-FG02-04ER54762, DE-FG02-04ER54758, and DE-AC05-00OR22725.

References

[1] T.H. Jensen, D.G. Skinner, Phys. Fluids B **2**, 2358 (1990).
[2] D.A. Humphreys and A.G. Kellman, Phys. Plasmas **6**, 2742 (1999).
[3] D.G. Whyte, et al., Phys. Plasmas **7**, 4052 (2000).
[4] D.A. Humphreys and D.G. Whyte, Phys. Plasmas **7**, 4057 (2000).
[5] D.G. Whyte, et al., Phys. Rev. Lett. **89**, 55001 (2002).
[6] D.L. Rudakov, et al., Nucl. Fusion **45**, 1589 (2005).